frontiers in Energy Research

ORIGINAL RESEARCH
published: 30 August 2016
doi: 10.3389/fenrg.2016.00032

Fabrication of All-Solid-State Lithium-Ion Cells Using Three-Dimensionally Structured Solid Electrolyte $Li_7La_3Zr_2O_{12}$ Pellets

*Mao Shoji, Hirokazu Munakata and Kiyoshi Kanamura**

Department of Applied Chemistry, Graduate School of Urban Environmental Sciences, Tokyo Metropolitan University, Tokyo, Japan

All-solid-state lithium-ion batteries using Li^+-ion conducting ceramic electrolytes have been focused on as attractive future batteries for electric vehicles and renewable energy conversion systems because high safety can be realized due to non-flammability of ceramic electrolytes. In addition, a higher volumetric energy density than that of current lithium-ion batteries is expected since the all-solid-state lithium-ion batteries can be made in bipolar cell configurations. However, the special ideas and techniques based on ceramic processing are required to construct the electrochemical interface for all-solid-state lithium-ion batteries since the battery development has been done so far based on liquid electrolyte system over 100 years. As one of the promising approaches to develop practical all-solid-state batteries, we have been focusing on three-dimensionally (3D) structured cell configurations such as an interdigitated combination of 3D pillars of cathode and anode, which can be realized by using solid electrolyte membranes with hole-array structures. The application of such kinds of 3D structures effectively increases the interface between solid electrode and solid electrolyte per unit volume, lowering the internal resistance of all-solid-state lithium-ion batteries. In this study, $Li_{6.25}Al_{0.25}La_3Zr_2O_{12}$ (LLZAl), which is a Al-doped $Li_7La_3Zr_2O_{12}$ (LLZ) with Li^+-ion conductivity of ~10^{-4} S ·cm^{-1} at room temperature and high stability against lithium-metal, was used as a solid electrolyte, and its pellets with 700 μm depth holes in 700 μm × 700 μm area were fabricated to construct 3D-structured all-solid-state batteries with $LiCoO_2$/LLZAl/lithium-metal configuration. It is expected that the $LiCoO_2$–LLZAl interface is formed by point-to-point contact even when the LLZAl pellet with 3D hole-array structure is applied. Therefore, Li_3BO_3, which is a mechanically soft solid electrolyte with a low melting point at around 700°C was also applied as a supporting Li^+-ion conductor to improve the $LiCoO_2$–LLZAl interface.

Keywords: all-solid-state lithium-ion battery, solid electrolyte, $Li_{6.25}Al_{0.25}La_3Zr_2O_{12}$, three-dimensional structure, Li_3BO_3

OPEN ACCESS

Edited by:
Fuminori Mizuno, Toyota Research Institute of North America, USA

Reviewed by:
Chunming Zhang, National Engineering Research Center for Nanotechnology, China
Pengjian Zuo, Harbin Institute of Technology, China

****Correspondence:***
Kiyoshi Kanamura
kanamura@tmu.ac.jp

Specialty section:
This article was submitted to Energy Storage, a section of the journal Frontiers in Energy Research

Received: *29 February 2016*
Accepted: *17 August 2016*
Published: *30 August 2016*

Citation:
Shoji M, Munakata H and Kanamura K (2016) Fabrication of All-Solid-State Lithium-Ion Cells Using Three-Dimensionally Structured Solid Electrolyte $Li_7La_3Zr_2O_{12}$ Pellets. Front. Energy Res. 4:32. doi: 10.3389/fenrg.2016.00032

INTRODUCTION

In recent years, the application of lithium-ion batteries has been expanded from portable electronic devices to large devices such as electric vehicles and energy storage systems on an industrial scale. According to this movement, higher battery performance, particularly safety is being required (Tarascon and Armand, 2001). However, it is basically difficult to realize high safety in current

lithium-ion batteries because of the use of liquid electrolytes including flammable organic solvents, which also demands the massive battery package to avoid the electrolyte leakage. Therefore, the replacement of liquid electrolytes with solid electrolytes is an important issue to contribute the improvement of both safety and energy density of lithium-ion batteries. Actually, these advantages can be confirmed in polymer lithium-ion batteries, however, in which gel-type electrolytes including liquid electrolytes have been still used owing to low conductivity of true polymer electrolytes. On the other hand, inorganic solid electrolytes have attracted much attention in recent decade since those materials are non-flammable and thermally stable (Knauth, 2009). So far, many kinds of inorganic solid electrolytes including both glass- and crystal-based materials have been developed. They are categorized into two major groups. One is sulfide-based solid electrolyte group, which mainly consists of glass materials with relatively high plasticity. In the recent development, the Li^+-ion conductivity of sulfide materials is approaching the value of liquid electrolytes. For example, 1.2×10^{-2} S cm^{-1} at room temperature has been reported for the composition of $Li_{10}GeP_2S_{12}$ by Kanno et al. (Kamaya et al., 2011). However, there is a serious problem to be solved. The sulfide-based solid electrolytes, particularly those with high Li^+-ion conductivity, easily react with water and generate toxic hydrogen sulfide gas. The other group consists of oxide-based solid electrolytes such as $Li_{0.35}La_{0.55}TiO_3$ (LLT), $Li_{1+x}Al_xTi_{2-x}(PO_4)_3$ (LATP), and $Li_7La_3Zr_2O_{12}$ (LLZ). Compared to the sulfide-based solid electrolytes, these kinds of solid electrolytes have good thermal and chemical stability and high mechanical strength. LATP has a NASICON-type (Na super ion conductor) structure and exhibits a total (bulk + grain-boundary) ionic conductivity of 7×10^{-4} S cm^{-1} at 25°C when the composition is $Li_{1.3}Al_{0.3}Ti_{1.7}(PO_4)_3$ (Aono et al., 1989, 1990). LLT is a perovskite-type oxide Li^+-ion conductor with a high bulk ionic conductivity of 1×10^{-3} S cm^{-1} at 25°C, but its total ionic conductivity is as low as 7.5×10^{-5} S cm^{-1} (Inaguma et al., 1993). These are not stable against Li-metal due to the reduction of Ti^{4+} to Ti^{3+} at 1.8 V vs. Li/Li^+, resulting in the appearance of electronic conduction (Knauth, 2009). Therefore, if lithium-metal is used as an anode in all-solid-state lithium-ion batteries to realize high energy density, a Li^+-conducting protective layer such as poly(methyl methacrylate) (PMMA) gel-electrolyte has to be formed as a buffer layer to prevent the direct contact of those solid electrolytes with Li-metal (Hoshina et al., 2005).

Recently, many research groups including our group are focusing on $Li_7La_3Zr_2O_{12}$ (LLZ) as one of promising solid electrolytes for all-solid-state lithium-ion batteries using Li-metal anode (Murugan et al., 2007a). LLZ has a wider electrochemical window than LLT due to the stability against Li-metal. The total ionic conductivity of LLZ with a cubic structure is 7.7×10^{-4} S cm^{-1} at 25°C, which is larger than that of LLT and also those of other Li^+-ion conducting garnet-like oxides (Thangadurai et al., 2003; Murugan et al., 2007b). In addition to the cubic phase, LLZ has a tetragonal phase, whose ionic conductivity is as low as ~10^{-6} S cm^{-1}. Therefore, it is necessary to use cubic LLZ for battery applications. The cubic phase is stable above 640°C and is easily transformed to the tetragonal phase as decreasing the temperature. Therefore, many approaches have been done to stabilize the cubic phase at room temperature. The Al^{3+} substitution of Li^+ sites in LLZ (Al-doping) is an effective way to improve the stability of cubic phase at room temperature. For example, $Li_{6.25}Al_{0.25}La_3Zr_2O_{12}$ ($x = 0.25$ in $Li_{7-3x}Al_xLa_3Zr_2O_{12}$) has been known as a stable cubic LLZ (Matsuda et al., 2015). These kinds of Al-doped LLZs are usually denoted as LLZAls and show a relatively high bulk ionic conductivity such as 3.1×10^{-4} S cm^{-1} at 25°C in $Li_{6.25}Al_{0.25}La_3Zr_2O_{12}$. Although the Li^+-ion conductivity of oxide-based solid electrolytes is still one order of magnitude lower than that of liquid electrolytes, a practical Li^+-ion conductivity similar to that of liquid electrolytes in a separator can be realized if those solid electrolytes are formed in the thickness of less than 50 μm since their Li^+-ion transport number is almost unity. In order to fabricate such thin solid electrolyte membranes with both high density and high mechanical strength, special fabrication techniques are required.

In our previous study, we fabricated a $LiCoO_2$ cathode layer on a LLZ pellet by a simple sintering process using $LiCoO_2$ powder at 800°C for 1 h. However, the electrochemical performance was very poor with the specific discharge capacity of as small as 0.27 mAh g^{-1} (Kotobuki et al., 2010). From the scanning electron microscopic observation, it was found that the contact between $LiCoO_2$ cathode and LLZ solid electrolyte was poor. This problem can be improved by applying the precursor sol of $LiCoO_2$. When the mixture of $LiCoO_2$ particles and its precursor sol is applied, the better electrode–electrolyte contact can be formed, resulting in the lower internal resistance of all-solid-state lithium-ion batteries (Kotobuki et al., 2011). A similar approach to improve the electrode–electrolyte contact in all-solid-state lithium-ion batteries has been carried out by Ohta et al. (2013). They applied Li_3BO_3 as a supporting electrolyte to improve the contact between $LiCoO_2$ cathode and LLZ solid electrolyte, in which the mixture of Li_3BO_3 and $LiCoO_2$ was sintered onto a LLZ pellet with the composition of $Li_{6.75}La_3(Zr_{1.75}Nb_{0.25})O_{12}$ optimized by them (Ohta et al., 2011). Consequently, the total resistance including $LiCoO_2$/LLZ and Li-metal/LLZ interfacial resistances was improved from 700 to 230 Ω cm^{-2}. This result suggests that the use of Li^+-ion conducting supporting electrolytes is effective to improve the solid (electrode)–solid (electrolyte) contact. However, the capacity of all-solid-state lithium-ion batteries cannot be increased only by the improvement of interfacial contact. It is basically needed to make thick electrodes to obtain high capacity in batteries. The Li^+-ion conductivity of cathode materials used in lithium-ion batteries are not so high. Therefore, thicker cathode layer for higher capacity cannot be used due to limit of the lithium-ion migration length. One of the ideas to realize practically high capacity in all-solid-state lithium-ion batteries is to make 3D-structured electrodes. Of course, this idea is applicable to current lithium-ion batteries using liquid electrolytes to improve their electrochemical performance. For example, the energy density of battery can be increased without losing the power density in the combination of interdigitated pillar-arrays of anode and cathode since the Li^+-ion diffusion length between anode and cathode can be maintained even when the electrodes

are made thicker (higher) to increase the battery capacity. Namely, the trade-off problem between energy and power density in batteries can be solved. Actually, we had reported this advantage by making some 3D-structured electrodes for current lithium-ion batteries (Izumi et al., 2012). The similar approach is also effective to increase the practical capacity of all-solid-state lithium-ion batteries. However, unlike liquid electrolytes, solid electrolytes have no fluidity, which makes it difficult to introduce them into the space between 3D-strucutrued electrodes. Oxide-based solid electrolytes have high mechanical strength compared to other electrolytes, so that their various 3D structures can be formed. When a solid electrolyte membrane with a hole-array structure is formed, 3D batteries can be fabricated by introduction of electrode active materials into the holes. In 3D-structured solid electrolyte membranes, the electrode–electrolyte contact area per unit volume is increased. Therefore, the application of 3D structures is particularly effective to improve the electrochemical performance of all-solid-state lithium-ion batteries. In addition, the electrolyte thickness in the bottom of holes can be thin for short Li^+-ion diffusion length since the other parts maintain the mechanical strength of electrolyte membrane. So far, we have tried to prepare LLZ solid electrolyte membranes with hole-array structures (**Figure 1**) by several methods. One is a micro-stereolithography using a LLZ slurry including a photo-curable resin. This method can make LLZ membranes with several tenths of micrometer-scale patterns precisely. However, their densification was difficult by simple sintering process (**Figure 2**). Consequently, the resulting LLZ membranes were porous and had high resistance. More simply, we recently have applied a press method using a die with a pillar-array structure to make LLZ pellets with a hole-array structure (Shoji et al., 2014). Compared to the micro-stereolithography, the fineness of patterns is slightly lost but dense LLZ pellets with 3D hole-array structures can be formed reproducibly. In this study, we apply this press method to make LLZAl pellets with 3D hole-array structures and present their effectiveness on improvement of electrochemical performance of all-solid-state lithium-ion batteries.

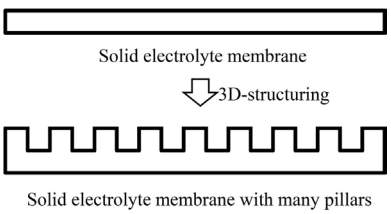

FIGURE 1 | Schematics of 3D-structured solid electrolyte membrane.

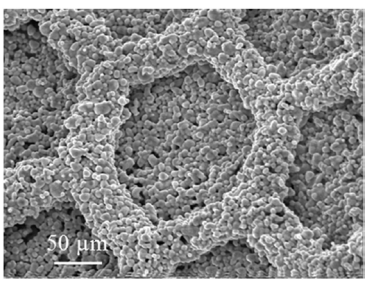

FIGURE 2 | SEM image of 3D-structured LLZ membrane.

MATERIALS AND METHODS

LLZAl powder was synthesized by a solid state reaction (Kotobuki et al., 2011). $LiOH{\cdot}H_2O$, $La(OH)_3$, ZrO_2 (7.7:3:2: in molar ratio) were mixed by planetary ball-milling and then calcined at 900°C for 6 h. The calcined powder was mixed with γ-Al_2O_3 powder by planetary ball-milling, and then a binder was added to make a pellet with a hole-array structure, i.e., 3D-structured pellet, by using a special punch, which has many small and short pillars (**Figure 3**). For comparison, a flat LLZAl pellet was also fabricated using binder-free powder. The 3D-structured pellet was sintered by two sintering steps of 900°C for 3 h and then 1200°C for 12 h. Although a sintering mechanism of LLZ is complicate, the two sintering steps can prevent to remain impurity phases such as $La_2Zr_2O_7$ and Li_2CO_3, which behave as an inhibitor of densifying LLZ (Chen et al., 2014).

The characterization of sintered 3D-structured LLZAl pellets was performed by X-ray diffraction (XRD) analysis, scanning electron microscopy (SEM), and impedance measurement from 0.1 to 10^6 Hz at 30°C. To estimate Li^+-ion conductivity of LLZAl, the 3D-structured LLZAl pellet was polished to be a flat pellet for removing the effect of 3D structure from the estimation of its Li^+-ion conductivity.

For the assembly of all-solid-state battery using the 3D-structured LLZAl pellet, $LiCoO_2$ cathode with and without Li_3BO_3 was filled into the holes of the 3D-structured LLZAl pellet. The detailed procedures are as follows: $LiCoO_2$ sol was prepared by mixing $LiNO_3$, $Co(NO_3)_2{\cdot}6H_2O$, CH_3COOH, 2-propanol, H_2O, and polyvinylpyrrolidone (PVP) in a molar ratio of 1.1:1:10:1:0.06. Li_3BO_3 powder was synthesized by a solid state reaction using Li_2CO_3 and B_2O_3 in a molar ratio of 3:1 (Ohta et al., 2013). For the case of $LiCoO_2$/Li_3BO_3 composite cathode, the mixture of $LiCoO_2$ sol and Li_3BO_3 in a weight ratio of 7:3 was injected into the holes of the 3D-structured LLZAl pellet. Then, it was calcination at 400°C for 5 min and then 700°C for

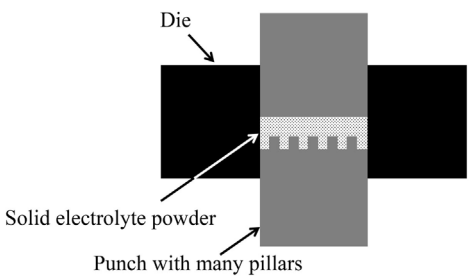

FIGURE 3 | Schematics of pelletization for 3D-structured pellet.

30 min to form an intermediate layer for making good contact between $LiCoO_2/Li_3BO_3$ composite cathode and LLZAl solid electrolyte. After that, the mixture of Li_3BO_3 powder and commercially available $LiCoO_2$ powder in a weight ratio of 3:7 was filled in holes of the 3D-structured LLZAl pellet, and then the Li_3BO_3-added $LiCoO_2$ sol denoted above was also dropped into the mixed powder-filled holes of the 3D-structured LLZAl pellet. This pellet was finally heated at 400°C for 5 min and then 700°C for 30 min. For comparison, Li_3BO_3-free sample was also prepared according to the same procedure except the use of Li_3BO_3. Their characterizations were performed by XRD, SEM, energy dispersive X-ray spectrometry (EDS), impedance measurement, and charge-discharge test.

RESULTS AND DISCUSSION

Figure 4 shows a photograph of sintered 3D-structured LLZAl pellet with a diameter of about 10 mm. The XRD pattern of the 3D-structured LLZAl pellet shown in **Figure 5** is attributed to the cubic crystal. From an impedance spectrum, the ionic conductivity of LLZAl estimated from its polished flat pellet was 3.5×10^{-4} S cm^{-1} at 30°C, which is a typical ionic conductivity of LLZ-type electrolytes. **Figure 6** shows surface and cross sectional SEM images of the 3D-structured LLZAl pellet. A pore size of holes on the 3D-structuerd LLZAl pellet was estimated to be about 700 μm × 700 μm. A thickness of the thick parts of 3D-structuerd LLZAl pellet and a depth of holes was about 1 mm and 700 μm, respectively. The electrolyte thickness in the bottom of holes was approximately 300 μm. This hole-array structure was very coarse. However, the surface area of the 3D-structuerd LLZAl pellet was approximately 2.5 times as large as flat pellet.

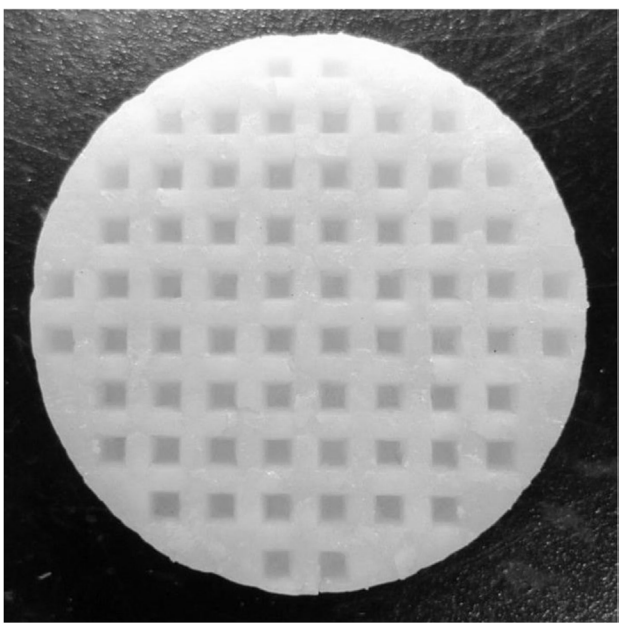

FIGURE 4 | Photograph of sintered 3D-structured LLZAl pellet with diameter of 10 mm.

In the 3D-structuerd LLZAl pellet, some large pores of about 100 μm and many small pores of about 10 μm were observed. The relative density of the 3D-structured LLZAl pellet was estimated to be 88.2%. A flat LLZAl pellet prepared from binder-free calcined powder had no large pores. Therefore, these large pores were formed by the use of calcined powder containing the binder. To get the large pores to disappear and improve the relative density, it is required to decrease the binder containing calcined powder and optimize a dewaxing process during the sintering. Only a few grain boundaries were observed in the 3D-structured LLZAl pellet. In our previous study (Shoji et al., 2014), we prepared a 3D-structured LLZAl pellet that contained many grain boundaries, and the all-solid-state battery using the 3D-structured LLZAl pellet did not work as a rechargeable

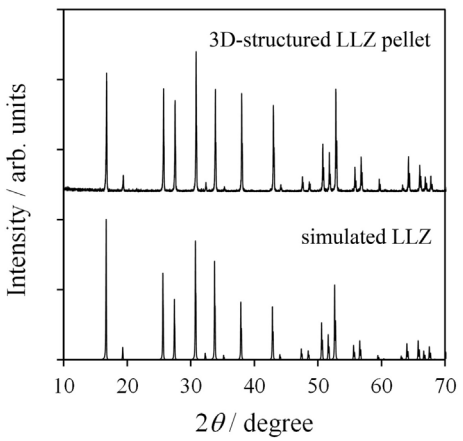

FIGURE 5 | XRD pattern of sintered 3D-structured LLZAl pellet and simulated cubic LLZ.

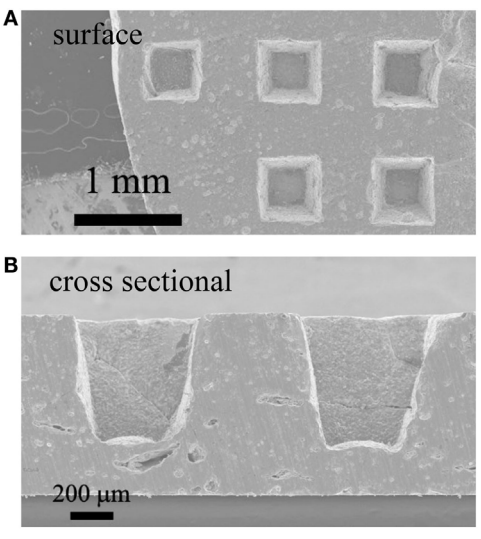

FIGURE 6 | (A) Surface and **(B)** cross sectional SEM images of 3D-structured LLZAl pellet.

battery. A two-sintering step process has not been adopted in the previous study. Therefore, the two-sintering step process has an effect on the decrement of grain boundaries by preventing impurity phases to remain. As a result, prepared 3D-structured LLZAl pellet in this study had no penetration. It was regarded that the 3D-structured LLZAl pellet can be used to fabricate the all-solid-state battery.

For improvement of contact between the $LiCoO_2$ layer and the 3D-structured LLZAl pellet, we used a Li_3BO_3 additive as a supporting electrolyte. Cross sections of each pellet were observed by SEM and EDS. These results are shown in **Figure 7**. By comparing these, large voids were not observed in the Li_3BO_3-added $LiCoO_2$ layer. However, the volumes of Li_3BO_3-added $LiCoO_2$ or Li_3BO_3-free $LiCoO_2$ layer except the voids were estimated to about the same, which were estimated from the amount of weight increment of the 3D-structured LLZAl pellets. The Li_3BO_3 additive has no work in densifying the $LiCoO_2$ layer. However, the Li_3BO_3-added $LiCoO_2$ layer was more uniformly distributed in the holes than Li_3BO_3-free $LiCoO_2$ layer. These results have indicated that the fluidity of $LiCoO_2$ layer emerged due to melting Li_3BO_3 around 700°C during the heat treatment, and then, $LiCoO_2$ in the holes was uniformly distributed. SEM images shown in **Figures 8B,C** clearly indicated that clay-like adhering material is attached around $LiCoO_2$ particles. Probably, this adhering material is Li_3BO_3 that is melted once during the heat treatment, and the Li_3BO_3 was connected to each $LiCoO_2$ particle and between $LiCoO_2$ particles and LLZAl. To confirm an effect of the Li_3BO_3 additive, an impedance measurement of each sample was carried out. Impedance spectra are showed in **Figure 9**. These spectra indicated a resistance of LLZAl (bulk and grain boundary) and interfacial resistances between LLZAl and electrodes (Li-metal and $LiCoO_2$), LLZAl and Li_3BO_3, and $LiCoO_2$ and Li_3BO_3. The resistances of bulk and grain boundary of LLZAl had no significant difference between each sample, about 0.2 kΩ. On the other hand, the interfacial resistances of the 3D-structured LLZAl pellet injected Li_3BO_3-added $LiCoO_2$ was lower than injected Li_3BO_3-free $LiCoO_2$. Since a Li-metal was not involved with Li_3BO_3, an interfacial resistance between LLZAl and Li-metal had no difference between each sample. Thus, $LiCoO_2$ and the Li_3BO_3 additive attributed to the decrement of the interfacial resistances, because the Li_3BO_3 additive can form a better contact in interface (Ohta et al., 2013).

Charge-discharge tests of all-solid-state lithium-ion batteries using the 3D-structured LLZAl pellets injected Li_3BO_3-free $LiCoO_2$ or Li_3BO_3-added $LiCoO_2$ were performed under a constant current density of 14 μA cm^{-2} in cutoff voltages of 2.5 and 4.2 V at 60°C. **Figure 10** shows charge–discharge curves of each sample. Both all-solid-state lithium-ion batteries were

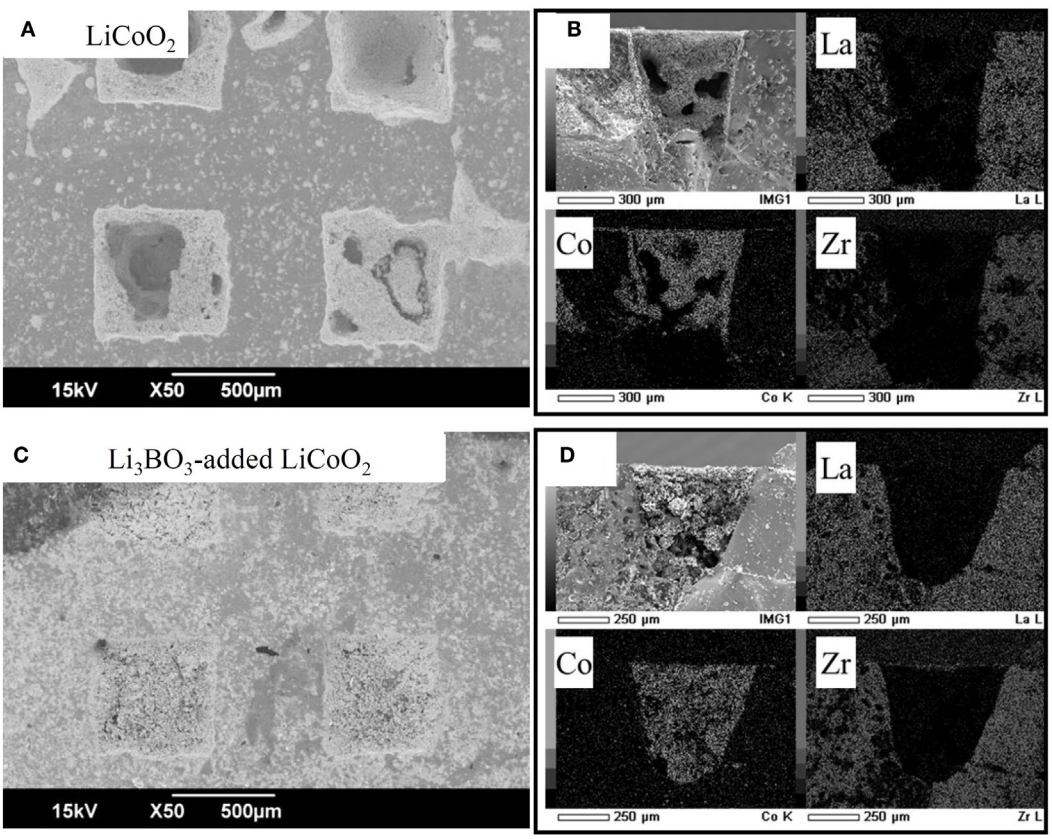

FIGURE 7 | SEM images and EDS mappings of 3D-structured LLZAl pellets injected Li_3BO_3-free $LiCoO_2$ (A,B) and $LiCoO_2$-Li_3BO_3 composite (C,D), respectively.

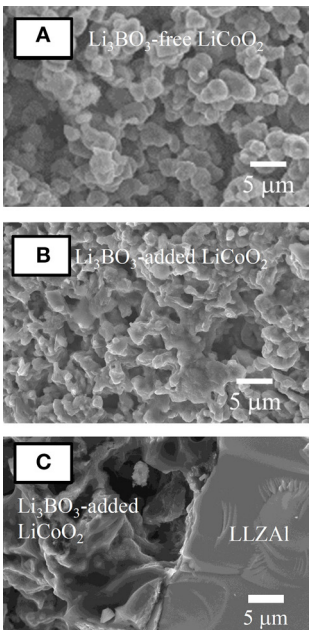

FIGURE 8 | SEM images (A) Li_3BO_3-free $LiCoO_2$, (B) Li_3BO_3-added $LiCoO_2$, and (C) interface between Li_3BO_3-added $LiCoO_2$ and LLZAl.

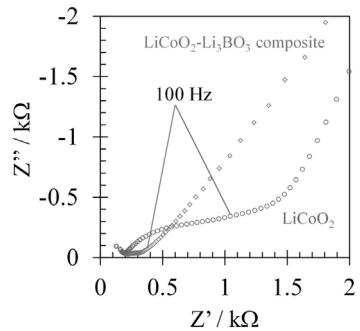

FIGURE 9 | Impedance spectra of $LiCoO_2$/flat LLZAl/Li-metal and $LiCoO_2$/3D-structured LLZAl/Li-metal batteries.

worked as rechargeable batteries, exhibiting very low discharge capacities between 0.6 ~ 7 mAh g^{-1}. On the other hand, the utilization of Li_3BO_3-added $LiCoO_2$ was larger than Li_3BO_3-free $LiCoO_2$. In the SEM images of **Figure 8**, each $LiCoO_2$ particle and $LiCoO_2$ and LLZAl pellet were connected by the Li_3BO_3 additive. It is considered that the improvement of the utilization was attributed to Li_3BO_3, which worked as ionic migration path. However, the utilization was still very low. It is attributed that the contact area between LLZAl and $LiCoO_2$ was still small. To improve the utilization, a denser Li_3BO_3-added $LiCoO_2$ layer is required. In addition, holes of the 3D-strucutred LLZAl pellet were too large for the Li^+-ion diffusion length. $LiCoO_2$ around the center of this large size holes could not be utilized as active materials due to too long of a distance between $LiCoO_2$ and

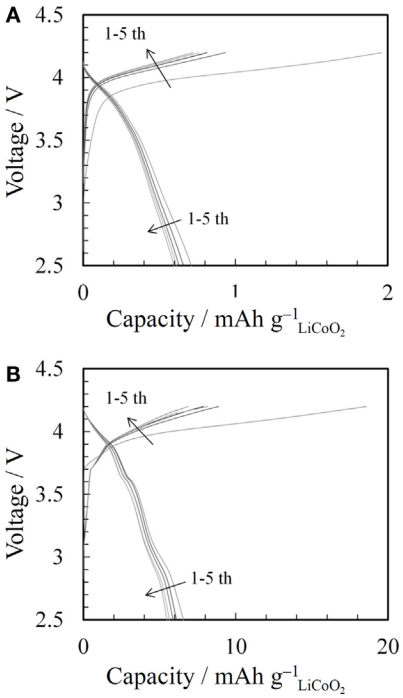

FIGURE 10 | Charge–discharge curves of (A) $LiCoO_2$/flat LLZAl/Li-metal and (B) $LiCoO_2$/3D-structured LLZAl/Li-metal batteries.

LLZAl. It is necessary to design finer hole with size of about 100 μm or less.

CONCLUSION

In this report, we reported about a concept of 3D-structuring of LLZAl solid electrolyte to realize high capacity density and high mechanical strength of all-solid-state lithium-ion batteries. Since densification of LLZAl membranes was difficult by simple sintering process, we made dense LLZAl pellets with 3D-structure (a hole-array structure). An ionic conductivity of the 3D-structured LLZAl was estimated to 3.5×10^{-4} S cm^{-1}, which is a sufficient ionic conductivity as a LLZ electrolyte. And it was confirmed that the all-solid-state battery using the 3D-structured LLZAl pellet was operated as a rechargeable battery. Also, addition of Li_3BO_3 to $LiCoO_2$ layer was an effective way to improve contact between each $LiCoO_2$ particles or $LiCoO_2$ and LLZAl. However, this battery could not exhibit high utilization of $LiCoO_2$ due to low density of $LiCoO_2$ layer and coarse holes of the 3D-structured LLZAl pellet. Finer hole-array structure with size of about 100 μm or less is required to improve a utilization of $LiCoO_2$. Of course, high mechanical strength is also needed. However, to realize the 3D-structured LLZAl membranes, it is necessary to establish techniques to mold using the punch with many finer pillars. Moreover, the optimization of sintering processes for preparation of dense LLZAl membranes must be studied.

AUTHOR CONTRIBUTIONS

KK conceived the conception and design of the study, MS performed the experiments and acquired the data, MS, HM and KK analyzed the data, MS and HM drafted and revised the manuscript.

ACKNOWLEDGMENTS

This work was supported by Advanced Low Carbon Technology Research and Development Program – Specially Promoted Research for Innovative Next Generation Batteries (ALCA-SPRING) from Japan Science and Technology Agency (JST).

REFERENCES

Aono, H., Sugimoto, E., Sadaoka, Y., Imanaka, N., and Adachi, G. (1989). Ionic conductivity of the lithium titanium phosphate ($Li_{1+x}M_xTi_{2-x}(PO_4)_3$, M = Al, Sc, Y, and La) systems. *J. Eectrochem. Soc.* 136, 590–591. doi:10.1149/1.2096693

Aono, H., Sugimoto, E., Sadaoka, Y., Imanaka, N., and Adachi, G. (1990). Ionic conductivity of solid electrolytes based on lithium titanium phosphate. *J. Eectrochem. Soc.* 137, 1023–1027. doi:10.1149/1.2086597

Chen, R.-J., Huang, M., Huang, W.-Z., Shen, Y., Lin, Y.-H., and Nan, C.-W. (2014). Effect of calcining and Al doping on structure and conductivity of $Li_7La_3Zr_2O_{12}$. *Solid State Ion.* 265, 7–12. doi:10.1016/j.ssi.2014.07.004

Hoshina, K., Dokko, K., and Kanamura, K. (2005). Investigation on electrochemical interface between $Li_4Ti_5O_{12}$ and $Li_{1+x}Al_xTi_{2-x}(PO_4)_3$ NASICON-type solid electrolyte. *J. Electrochem. Soc.* 152, A2138–A2142. doi:10.1149/1.2041967

Inaguma, Y., Liquan, C., Itoh, M., Nakamura, T., Uchida, T., Ikuta, H., et al. (1993). High ionic conductivity in lithium lanthanum titanate. *Solid State Commun.* 86, 689–693. doi:10.1016/0038-1098(93)90841-A

Izumi, A., Sanada, M., Furuichi, K., Teraki, K., Matsuda, T., Hiramatsu, K., et al. (2012). Development of high capacity lithium-ion battery applying three-dimensionally patterned electrode. *Electrochim. Acta* 79, 218–222. doi:10.1016/j.electacta.2012.07.001

Kamaya, N., Homma, K., Yamakawa, Y., Hirayama, M., Kanno, R., Yonemura, M., et al. (2011). A lithium superionic conductor. *Nat. Mater.* 10, 682–686. doi:10.1038/nmat3066

Knauth, P. (2009). Inorganic solid Li ion conductors: an overview. *Solid State Ion.* 180, 911–916. doi:10.1016/j.ssi.2009.03.022

Kotobuki, M., Munakata, H., Kanamura, K., Sato, Y., and Yoshida, T. (2010). Compatibility of $Li_7La_3Zr_2O_{12}$ solid electrolyte to all-solid-state battery using Li metal anode. *J. Electrochem. Soc.* 157, A1076–A1079. doi:10.1149/1.3474232

Kotobuki, M., Suzuki, Y., Munakata, H., Kanamura, K., Sato, Y., Yamamoto, K., et al. (2011). Effect of sol composition on solid electrode/solid electrolyte interface for all-solid-state lithium ion battery. *Electrochim. Acta* 56, 1023–1029. doi:10.1016/j.electacta.2010.11.008

Matsuda, Y., Sakamoto, K., Matsui, M., Yamamoto, O., Takeda, Y., and Imanishi, N. (2015). Phase formation of a garnet-type lithium-ion conductor $Li_{7-3x}Al_xLa_3Zr_2O_{12}$. *Solid State Ion.* 277, 23–29. doi:10.1016/j.ssi.2015.04.011

Murugan, R., Thangadurai, V., and Weppner, W. (2007a). Fast lithium ion conduction in garnet-type $Li_7La_3Zr_2O_{12}$. *Angew. Chem. Int. Ed.* 46, 7778–7781. doi:10.1002/anie.200701144

Murugan, R., Thangadurai, V., and Weppner, W. (2007b). Lithium ion conductivity of $Li_{5+x}Ba_xLa_{3-x}Ta_2O_{12}$ (x=0–2) with garnet-related structure in dependence of the barium content. *Ionics* 13, 195–203. doi:10.1007/s11581-007-0097-8

Ohta, S., Kobayashi, T., and Asaoka, T. (2011). High lithium ionic conductivity in the garnet-type oxide $Li_{7-X}La_3(Zr_{2-X}, Nb_X)O_{12}$ (X = 0–2). *J. Power Sources* 196, 3342–3345. doi:10.1016/j.jpowsour.2010.11.089

Ohta, S., Komagata, S., Seki, J., Saeki, T., Morishita, S., and Asaoka, T. (2013). All-solid-state lithium ion battery using garnet-type oxide and Li_3BO_3 solid electrolytes fabricated by screen-printing. *J. Power Sources* 238, 53–56. doi:10.1016/j.jpowsour.2013.02.073

Shoji, M., Wakasugi, J., Osone, R., Nishioka, T., Munakata, H., and Kanamura, K. (2014). "Design and fabrication of all-solid-state rechargeable lithium batteries for future applications," in *Proceedings of the 38th International Conference on Advanced Ceramics and Composites Jan 26–31* (Daytona Beach, FL: The American Ceramic Society).

Tarascon, J.-M., and Armand, M. (2001). Issues and challenges facing rechargeable lithium batteries. *Nature* 414, 359–367. doi:10.1038/35104644

Thangadurai, V., Kaack, H., and Weppner, W. J. F. (2003). Novel fast lithium ion conduction in garnet-type $Li_5La_3M_2O_{12}$ (M = Nb, Ta). *J. Am. Ceram. Soc.* 86, 437–440. doi:10.1111/j.1151-2916.2003.tb03318.x

Conflict of Interest Statement: The authors declare that the research was conducted in the absence of any commercial or financial relationships that could be construed as a potential conflict of interest.